



Analysis of manufacturing and material parameters in 3D-printed polylactic acid (PLA) parts filled with glass powder: mechanical, economic, and environmental assessment

Laura Castanon-Jano^{1,2} · Paula Palomera-Obregon^{1,2} · Elena Blanco-Fernandez² · Irune Indacoechea-Vega²

Received: 4 May 2023 / Accepted: 21 July 2023 / Published online: 31 July 2023
© The Author(s) 2023

Abstract

This study investigates the influence of the addition of glass powder, nozzle size, and infill density on the mechanical properties of 3D-printed polylactic acid (PLA) pieces. To do so, a factorial design of experiments was accomplished. The specimens were tested under tensile and bending conditions. Regression equations were extracted from the maximal strength, strain at maximal strength and modulus, and an analysis of the significance of the terms was carried out. All the factors influence the output variables, independently and in combination. As for the environmental impact, a cradle-to-gate life cycle analysis (LCA) of the printing material with different glass powder additions, including the manufacturing process and transportation of the raw materials, was performed. Additionally, a cost assessment of each alternative was calculated for each case. Since the concurrence of mechanical, environmental, and cost performance is needed to enter a new product in the industry, a multicriteria decision-making analysis was performed to select the best combination. The criteria considered were the material and printing costs and the environmental impact, all normalized with maximal strength. Two different alternatives were found to be the best solution depending on the strength selected. Both of them were printed using a 1.2-mm nozzle with 100% infill and different glass percentages.

Keywords 3D printing · Design of experiments · Tension · Bending · Life cycle analysis · Multicriteria decision making analysis

1 Introduction

Additive manufacturing (also called 3D printing) of plastics has become an increasingly common and popular technology. With a variety of 3D printing processes available for a wide range of materials, this manufacturing technology has been widely adopted in a large number of fields, including mechanical engineering, civil engineering, aerospace, electronics, and biomedical [1, 2]. Among all the types of additive manufacturing is the fusion deposition modeling

(FDM) technology [3], which is based on the creation of objects by depositing layers of molten thermoplastic polymers starting from a spooled filament. This process starts with pre-processing, continues with the construction of the piece itself and ends with post-processing if necessary. In the pre-processing, the CAD geometry of the part to be manufactured is divided into layers, and the printing parameters of the process are established. Then, the piece is built in the 3D printer, where the filament is molten, extruded, and deposited layer by layer until the piece is complete. If there is any support, it will be removed in the post-processing phase. This technology started out being used for rapid prototyping and proofs of concept, but over the years, it has gained more weight in other fields due to the low price of machinery and materials in relation to other types of additive manufacturing.

The printing parameters defined in the pre-processing will determine, among other characteristics, the mechanical behavior of the printed part. For this reason, numerous authors have dedicated to investigate the parameters considered most relevant:

✉ Laura Castanon-Jano
laura.castanon@unican.es

¹ Area of Manufacturing Processes, School of Industrial Engineering and Telecommunications, University of Cantabria, Avda de los Castros S/N, 39005 Santander, Spain

² GITECO Research Group, School of Civil Engineering, University of Cantabria, Avda de los Castros S/N, 39005 Santander, Spain

infill pattern [4, 5], orientation of the layers [6, 7], printing speed [8–10], printing temperature [8, 11, 12], the thickness of the layers [5, 8, 13], or the infill density [4, 5, 13, 14].

Regarding the materials used in FDM, the most frequent for having more aptitudes for printing are PLA (polylactic acid [13–16]), ABS (acrylonitrile butadiene styrene) [14], or PETg (polyethylene terephthalate glycol) [15]. In recent years, all countries have reached a unanimous decision to reduce the amount of plastic waste generated or to look for fewer polluting alternatives, steering towards biodegradable or recycled materials. In this line, PLA is not made from fossil fuels and is degradable under certain environmental conditions, which is why it is considered the most environmentally friendly printable polymer. Lately, the possibility of adding or substituting a percentage of the polymer for another material in the form of powder or fibers has also been extensively studied by many authors seeking two objectives: reduce the amount of plastic used and try to improve some properties of the final product. These additions can be in the form of metallic powder [17–20], nut shells [21, 22], seashells [23–25], textile fibers [26, 27], or glass [28, 29].

In general, any work that falls within the scope of 3D plastics manufacturing should pursue three main objectives:

- *Minimization of the amount of material to be used:* the interest lies in knowing how the mechanical properties vary when reducing the amount of material to be used; that is, replacing a completely solid piece with one with a partially hollow one, modifying the printing parameter called “infill density.”
- *Reduction of printing time:* plastic 3D printers usually have by default nozzle sizes of 0.4 mm in diameter. However, this is especially intended for manufacturing parts dimensions no larger than $15 \times 15 \times 15 \text{ mm}^3$. This means that the printing time would be very high on parts with large volumes but could be reduced by using larger nozzle diameters. Therefore, there is a need to evaluate the mechanical properties of printed parts using the largest nozzle sizes found on the market for the printer available.
- *Promotion of the circular economy:* among the thermoplastics employed in 3D printing, PLA is the most environmentally friendly alternative. In addition, the use of powder fillers from waste from other production processes enhances the circular economy. Specifically, in this work, glass powder with a particle size between 0.05 and 0.4 mm is available.

Some of these parameters have already been analyzed in other works, although as suggested and demonstrated by Ruben Bayu Kristiawan et al. [30], the relationships between factors and parameters are still unclear and should be investigated.

Authors such as Rodriguez-Panes et al. [14] and Algarni et al. [31] studied the influence of numerous printing parameters and concluded that the percentage of filler is the most influential on the mechanical properties of the materials evaluated, so it is important to quantify this influence according to the characteristics of the material and the rest of the printing parameters.

On the other hand, there is hardly any information related to the nozzle size used in the process. Only Alsoufi et al. [32] and Ferretti et al. [33] study the change in nozzle diameter with respect to the roughness of the surfaces built and the volume of defects generated, respectively. Thus, it is necessary to analyze the change of the mechanical parameters with a nozzle diameter.

In relation to the use of glass powder added to the polymeric base, there are hardly any studies analyzing the strength, and the existing ones suggest a slight worsening of the mechanical properties [29], which should be further studied. The added value of this analysis lies on the simultaneous study of the three parameters so that the results reveal not only the influence of these parameters independently but also the interaction among them.

Considering the above, this paper firstly focuses on the evaluation of the influence of infill density, nozzle size, and the addition of glass powder to the PLA polymeric based on the tensile and flexural mechanical properties. This will be done among the different cases generated from the parameter combination.

Secondly, once the mechanical parameters are obtained, the other two criteria that are fundamental for the future market uptake of the technology and the materials will be assessed: economic and environmental aspects of the different cases mentioned.

It is vital that the results obtained from these three aspects are considered when it comes to industrialize a process. Having this into account, and in order to decide the most suitable case from the ones studied, a multi-criteria analysis (MCDMA) is used that will encompass the most relevant aspects in this decision.

2 Materials and methods

2.1 Materials

The PLA was supplied in pellets shape by the company EOLAS Prints (Cantabria, Spain). Glass powder, which comes from the shredding of car windows, was supplied by the waste management company FCC Ámbito S.A. (Cantabria, Spain) and was used as an additive. After crushing, the coarser fraction can be re-melted and used to produce more glass. However, this is not feasible for the finer fraction that is usually recycled in other

applications (i.e., ceramic industry and construction materials). After carrying out 3D printing work on concrete incorporating this material [34, 35], it was decided to also incorporate it into the FDM 3D printing process for plastic, specifically PLA in this case, in order to analyse its behaviour.

2.2 Design of experiments

The first handicap lies in finding the right number of experiments to carry out this study with precision. To this end, it was decided to use a design of experiments (DoE), a statistical tool that rationalises the number of tests to work out, afterwards, correlations, or regression models. It is therefore used to design the ideal conditions of a product, process, or service so that it meets the expectations placed on it by using a minimum number of trials and tests. Specifically, a 3-factor full factorial design with a central point was used. This results in a total of 9 combinations, which are shown in Table 1. Minimum and maximum values must be given to each parameter. In this case, the following:

- Nozzle size (mm): this value is directly related to the printing speed, so its increment leads to a desirable manufacturing time reduction. Taking these into account and considering the model of the printer available for this research, large nozzle size values were aimed to be used. Hence, the largest nozzle size used was 1.2 mm, and the minimum was 0.8 mm. Selecting these two values allows to include a central point (1 mm).
- Infill density (%): a completely solid piece exhibits the highest level of strength, while reducing the infill density leads to a decrease in resistance. However, minimizing the amount of material used is desirable to mitigate costs and environmental impact. Therefore, the infill density is selected to be at its maximum value of 100%, representing a solid piece, while

a minimum of 80% is deemed acceptable to reduce material usage without compromising the resistance of the component.

- Weight percentage of glass powder added to PLA (%): the maximum selected value was 10% glass, which was found appropriate for obtaining filament with correct diametrical tolerances and uniform filament diameter along the spool. The minimum was a 0%, that is, virgin PLA, as a reference to compare with.

The central point corresponds to the intermediate values of the three parameters: 1 mm of nozzle size, 90% infill density, and 5% of glass content. Each case was reproduced in a total of 5 replicates, as indicated in the test standards, detailed in Section 2.5. Therefore, a total of 45 experiments for each type of test were performed, that is, 45 for tension and 45 for bending.

2.3 Filament manufacturing

The filament was manufactured using pure PLA or a mixture of PLA with glass powder in the percentage defined for each case, using the 3devo Composer 450 desktop extruder (Fig. 1a). The equipment has a single extrusion screw with a geometry specially designed to make mixtures of plastic and other powder components thanks to the grooved shape of its end part. It has a small hopper where the material is deposited. It passes through a grid into the extrusion screw, which operates at four different temperatures at four different points along its longitudinal direction. The temperatures used in this work, ordered from the beginning to the end of the extrusion screw are 170, 185, 190, and 170 °C. Subsequently, the extruded material exits through the nozzle, where it is cooled by two fans and the diameter is controlled by a sensor incorporated into the machine. Finally, the extruder itself also has a winding system for the extruded product, which adapts to the output speed of the material.

Prior to the extrusion process, the PLA was dried at 60 °C for 24 h to remove as much moisture as possible and minimise the appearance of pores in the filament.

2.4 3D Printing of specimens

The machine used to manufacture the samples was the Artillery Sidewinder X1 3D printer (Fig. 1b). The software used for the pre-processing was Ultimaker Cura, in which the specimens (Fig. 1b) are imported in STL format, placed on the bed, and the printing parameters are defined.

Table 2 shows the parameters that have been kept constant in all the cases studied. The modification of the nozzle

Table 1 Analyzed cases of factorial DoE

| Case | % glass | Nozzle size (MM) | % infill |
|------|---------|------------------|----------|
| 1 | 0 | 0.8 | 80 |
| 2 | 10 | 0.8 | 80 |
| 3 | 0 | 1.2 | 80 |
| 4 | 10 | 1.2 | 80 |
| 5 | 0 | 0.8 | 100 |
| 6 | 10 | 0.8 | 100 |
| 7 | 0 | 1.2 | 100 |
| 8 | 10 | 1.2 | 100 |
| 9 | 5 | 1 | 90 |

Fig. 1 **a** 3devo Composer 450 extruder and **b** 3D printer Artillery Sidewinder X1

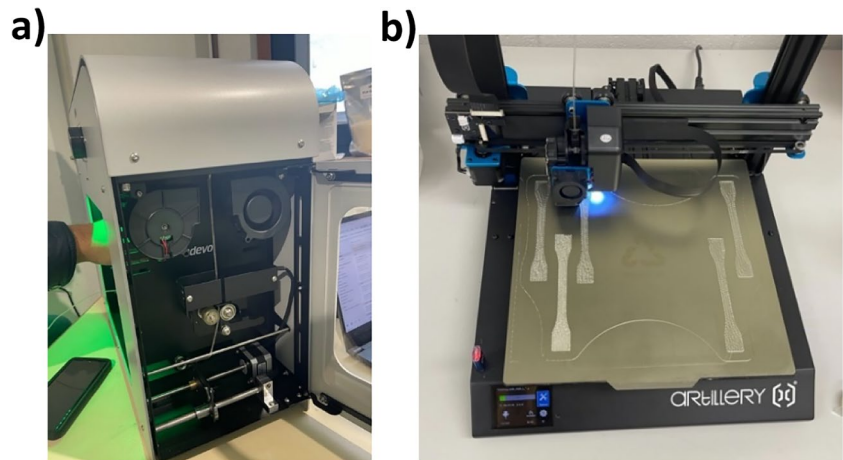


Table 2 Parameters of all the printed parts

| Parameters | Magnitude |
|-------------------------|-------------|
| Layer height | 0.4 mm |
| Number of contour lines | 1 |
| Printing temperature | 200 °C |
| Bed temperature | 40 °C |
| Printing speed | 45 mm/s |
| Contour speed | 30 mm/s |
| Retraction distance | 0.2 mm |
| Retraction speed | 25 mm/s |
| Infill line directions | [45°, -45°] |
| Build orientation | Horizontal |

size according to the case under consideration affects the parameter called “Line Width,” this being equal to the nozzle diameter; i.e., 0.8, 1 or 1.2. The other parameter to be modified is called “Infill Density,” which is replaced by 100%, 80%, or 90% depending on the percentage to be evaluated.

2.5 Tension and flexural tests

Tension tests were performed according to UNE-EN ISO 527–2:2019 [36]. Type 1B specimen geometry was chosen, with a halter shape. In the case of the bending specimens, the standard UNE-EN-ISO 178:2019 [37], whose specimens have a prismatic geometry, was used.

Both tests were carried out on a Zwick Roell Z100 universal testing machine. The tension tests were performed by clamping the ends of the specimens between two flat grips leaving a specimen base test length of 115 mm, while the base length between optical gauges to measure

deformations was set to 50 mm. Bending tests were carried out over an 80 mm length × 10 mm width specimen, 64 mm separation between supports, and a punctual load applied at the center of the specimen.

2.6 Life cycle assessment (LCA)

A cradle-to-gate life cycle assessment was carried out to assess the impact on the environment of each alternative as described on Table 1. The Life Cycle Inventory was performed with Ecoinvent 3.0 database and the Impact Assessment according to the Environmental Footprint Methodology (EF 3.0). Thus, sixteen impact categories were considered in the LCA, which are listed in Section 3.3.

2.7 Costs

The calculation of the costs was divided in filament and in printing cost. Filament cost involves the sum of the materials (PLA pellets and glass powder) as well as the extrusion costs. Extrusion costs were calculated according to Eq. 16 dividing the depreciation and maintenance cost of the extruder by the mass flow estimated experimentally:

$$\text{Filament extrusion cost} = \frac{\frac{C-SV}{SL} + \frac{CR_{\text{annual}}}{H_{\text{annual}}}}{\dot{m}} \quad (1)$$

where C is the cost of the extruder in €, SV is the saved value in €, SL is the shelf life of the extruder in hours, H_{annual} is the annual use in hours, and \dot{m} is the mass flow in kilograms per hour. The printing cost was obtained as the sum of the price of depreciation and maintenance of the machine, as well as the electricity supplies and labor costs associated with the printing time for each case. Depreciation and maintenance cost of the printer were calculated in the same way as for the extrusion, using Eq. 1, and substituting the data of the extruder by the one of the 3D printer.

2.8 Multicriteria decision-making analysis

As anticipated in the introduction (Section 1), the achievement of certain mechanical characteristics is not the only objective of the work. Due to the appearance of more than one criterion in the decision-making process and the non-uniformity between the weights of these criteria, it was decided to use the multi-criteria decision-making analysis (MCDMA). The weighting of the criteria was performed using AHP (analytical hierarchy process) [38], while the alternatives were assessed by two different techniques: WASPAS (weighted aggregated sum product assessment) [39] and TOPSIS (technique for order preference by similarity to ideal solution) [40].

2.8.1 Selection of criteria

From a commercial point of view, there are three main criteria that influence the decision on the best alternative: filament cost, printing cost, and environmental impact. Considering that parts will be manufactured for structural purposes, strength cannot be left as an isolated criterion, but must be integrated into the above-mentioned criteria. This is because the aim is to reduce costs and environmental impact related to strength as much as possible. Thus, a normalization was made by dividing each criterion by the strength in MPa. Due to the fact that results have been obtained through tests of two types, four MDMA were carried out, two (one WASPAS and one TOPSIS) normalizing with the tensile strength and the other two (WASPAS and TOPSIS) with the flexural strength.

The selected criteria were the following:

- Filament cost ((€/kg)/MPa): this parameter evaluates the cost of the filament per unit mass used in each case, normalized by the resistance. PLA with glass powder in different proportions was used as the material to produce the filament.
- Printing cost ((€/kg)/MPa): as in any manufacturing processes, in 3D printing is vital to minimise the production time, which leads to a reduction in the printing cost (amortization of machines, labor, and supplies). The production time of the parts depends directly on the printing parameters used. This criterion is where the influence of the nozzle size and the infill density was considered, as these have a direct impact on the printing time. The printing cost was evaluated by normalizing by the respective strength.
- Environmental impact ((LCA/kg)/MPa): the incorporation of glass powder has a positive effect on the circular economy, since a new recycling route is given for this material whose reuse is not feasible. The environmental impact was measured by a life cycle assessment (LCA), which provides a numerical value dependent on 28 indicators, and was also normalized by the strength.

2.8.2 Selection of alternatives

The alternatives assessed correspond to the 9 DoE cases defined in Section 2.2. These cases differ in the infill density (and therefore, the amount of material used), nozzle size (which has an impact on manufacturing time and consequently costs), and percentage of glass (enhancing the circular economy in those cases where glass is used, thus reducing the environmental impact of the solution).

2.8.3 Weighting the criteria: AHP

This analytic hierarchy process (AHP) is based on the scoring of criteria by comparing them two by two [38]. Saaty proposes a relative importance scale in which he specifies that values are scored on a range from 1 to 9, from giving them equal importance to giving extreme importance to one against the other (Table 3).

The pairwise comparison matrix of Eq. 2 is constructed using this range of values. The values of the diagonal take value 1 (thus expressing that a criterion is compared with itself, having the same importance), and the value it gives when comparing criterion j with criterion i (a_{ji}) must be the inverse of the one obtained when comparing criterion i with j (a_{ij}).

$$A = \begin{bmatrix} a_{11} & \dots & a_{1j} & \dots & a_{1n} \\ \vdots & & \vdots & & \vdots \\ a_{i1} & \dots & a_{ij} & \dots & a_{in} \\ \vdots & & \vdots & & \vdots \\ a_{n1} & \dots & a_{nj} & \dots & a_{nn} \end{bmatrix}, a_{ii} = 1, a_{ij} = \frac{1}{a_{ji}}, a_{ji} \neq 0 \quad (2)$$

Next, matrix A is normalized. This is done by dividing each value of the matrix by the sum of the values of the same column.

$$\bar{a}_{ij} = \frac{a_{ij}}{\sum_{l=1}^n a_{lj}} \quad (3)$$

Finally, the vector weight is obtained. This is calculated with the average of all the values of the same row.

$$w_i = \frac{\sum_{l=1}^n \bar{a}_{il}}{n} \quad (4)$$

Table 3 Saaty’s scale of relative importance

| Level of importance | Linguistic term |
|---------------------|---------------------|
| 1 | Equal |
| 3 | Moderate |
| 5 | Strong |
| 7 | Very strong |
| 9 | Extreme |
| 2, 4, 6, and 8 | Intermediate values |

2.8.4 Weighting the alternatives

WASPAS With the combination of the weighted sum model (WSM) and the weighted product model (WPM), the weighted sum of products assessment (WASPAS) is obtained. This is one of the most robust MCDMA methods and was developed by Zavadskas et al. 2012 [39].

To perform the calculation with the WASPAS method, the following steps should be followed:

- a) First, the weighted decision matrix for both criteria (beneficial and non-beneficial) should be normalized. A criterion is beneficial if its value is desired to be as high as possible, while if the best option is to be as low as possible, it is a non-beneficial criterion. Equations (4) and (5) are used for normalization.

$$X'_{ij} = \frac{X_{ij}}{\max(X_{ij})} \rightarrow \text{Beneficial} \quad (5)$$

$$X'_{ij} = \frac{\min(X_{ij})}{X_{ij}} \rightarrow \text{Non – beneficial} \quad (6)$$

- b) Then, the total relative importance is calculated by means of the following:

- The weighted sum model (WSM): it is defined as the sum of the product of the weight in column j (W_j) plus the values that were normalized in the previous point.

$$A_i^{\text{WSM}} = \sum_{j=1}^n W_j \cdot X'_{ij} = Q_i^1 \quad (7)$$

- The weighted product model (WPM): this is the sum of normalized values boosted by the weight of the criteria.

$$A_i^{\text{WPM}} = \prod_{j=1}^n X'^{W_j}_{ij} = Q_i^2 \quad (8)$$

- c) The weighted aggregation of both the additive and multiplicative methods is used as a generalized criterion. Thus, the relative importance of each alternative is obtained, with the Eq. 8.

$$Q_i = 0.5Q_i^1 + 0.5Q_i^2 \quad (9)$$

TOPSIS The technique of order preference by similarity to ideal solution (TOPSIS) tries to select in a way that chooses the shortest distance to the positive ideal solution and the farthest distance to the negative ideal solution [40].

The steps to follow the TOPSIS method are as follows:

- a) Dividing each value by the square root of the sum of the squared vertical values, the decision matrix is normalized.

$$r_{ij} = \frac{X_{ij}}{\sqrt{\sum_{i=1}^n X_{ij}^2}}, \quad i = 1, 2, \dots, n; j = 1, 2, \dots, m \quad (10)$$

- b) Then, multiplying each value of the normalized matrix (r_{ij}) by its weights (w_j) to obtain the weighted normalized decision matrix.

$$V = (v_{ij})_{m,n} \quad (11)$$

$$v_{ij} = w_j r_{ij}, \quad i = 1, 2, \dots, n; j = 1, 2, \dots, m$$

- c) The ideal solution is determined using Eq. (12) and the negative ideal solution using Eq. 13, considering the beneficial criteria set Ω_b and non-beneficial criteria set Ω_c .

$$V_j^+ = \{v_1^+, \dots, v_2^+\} = \left\{ \max_j v_{ij} | j \in \Omega_b \right\}, \left\{ \min_j v_{ij} | j \in \Omega_c \right\} \quad (12)$$

$$V_j^- = \{v_1^-, \dots, v_2^-\} = \left\{ \min_j v_{ij} | j \in \Omega_b \right\}, \left\{ \max_j v_{ij} | j \in \Omega_c \right\} \quad (13)$$

- d) The Euclidean distances of each alternative from the positive ideal solution and the negative ideal solution are calculated using Eqs. 14 and 15.

$$S_i^+ = \left(\sum_{j=1}^m (V_{ij} - V_j^+)^2 \right)^{0.5} \quad (14)$$

$$S_i^- = \left(\sum_{j=1}^m (V_{ij} - V_j^-)^2 \right)^{0.5} \quad (15)$$

- e) The relative closeness of each alternative to the ideal solution is reached.

$$P_i = \frac{S_i^-}{S_i^+ + S_i^-} \quad (16)$$

3 Results and discussion

3.1 Mechanical tests

For each specimen, the stress vs. strain curve was obtained in the case of tension, or force vs. deflection in the case of bending. From these, calculations using equations on the standards UNE-EN ISO 527–2:2019 [36] and UNE-EN-ISO 178:2019 [37] were made for the variables of interest:

maximum strength (σ), elastic modulus (E), and strain at the point of maximum strength (ϵ). Table 4 shows the mean values and percentage deviations of the five replicates of each DoE case for each of the six mechanical outputs. Some results were discarded due to problems during the test (premature breakage or breakage in the jaw area) or results that were markedly abnormal with respect to the rest of the specimens in the same case (outliers).

It was decided to analyze the strain variable at the point of maximum strength instead of at the breaking point after creep, since the purpose of this material is to have a function that is not only aesthetic but also resistant, so it is necessary to avoid working in the creep zone. In addition, the breakage in tension occurs violently and close to the point of maximum resistance, with hardly any travel, so that both deformations are not far from each other. This does not occur in bending, since it can be seen (Fig. 2) that, after the maximum strength, the increase in strain produces a significant reduction in the stress until breakage, a zone in which it is not advisable to work in the use of these materials.

3.2 DoE statistical evaluation

The regression equations obtained for each variable are shown in Table 5. Minitab software was chosen for the DoE and statistical evaluation, including the regression equations. The data of the five replicas were introduced on the software for the analysis.

In the analysis of the tensile behavior, it is observed that the regression equations obtained for the variables elastic modulus and strength are capable of correctly reproducing the behavior according to their influential parameters in each case since they show a predictive R^2 of more than 89%. However, in relation to the case of the tensile strain equation, the model has low fitting values. This lack of fit can be assigned to two causes:

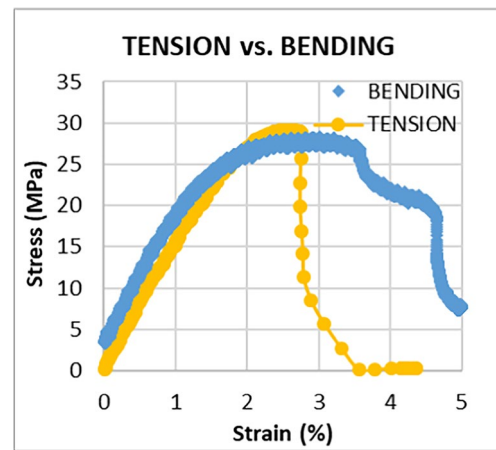


Fig. 2 Differences in the strain and the plastic zone of bending and tension tests (case 3)

- I. The way in which the load is applied in both tests causes tensile failure to be more abrupt compared to bending, and there are cases in tension where failure occurs even before the curve of the material reaches its maximum. In the case where the stress reaches its maximum point, the breakage occurs immediately afterwards. This can certainly distort the tensile results, having more influence on the strain than on the strength, since close to the failure point the curve flattens. Consequently, a high increment of strain leads to a low growth of stress. On the contrary, in bending tests, the maximum is recorded in all cases, since there is a notably greater difference between the point of maximum strength and the point of breakage of the part. Thus, the bending plastic zone is much larger than the tensile plastic zone. In particular, as shown in Fig. 2 for case 3, the plastic zone in bending is approximately 83% larger than that in tension. This situation can be extrapolated to the rest of the cases.

Table 4 Results (strength, elastic modulus, and strain) of the tension and bending tests on the 9 DoE cases

| Case | G (%) | \varnothing_{nozz} (mm) | I (%) | Tension | | | Bending | | |
|------|---------|---------------------------|---------|------------------|---------------|------------------|------------------|-------------|------------------|
| | | | | σ_t (MPa) | E_t (MPa) | ϵ_t (%) | σ_f (MPa) | E_f (MPa) | ϵ_f (%) |
| 1 | 0 | 0.8 | 80 | 24.05 ± 2% | 1285.71 ± 6% | 2.72 ± 11% | 37.82 ± 1% | 1423.2 ± 4% | 4.78 ± 9% |
| 2 | 10 | 0.8 | 80 | 22.19 ± 4% | 1304.20 ± 9% | 3.07 ± 19% | 38.55 ± 4% | 1455 ± 3% | 4.62 ± 6% |
| 3 | 0 | 1.2 | 80 | 29.53 ± 2% | 1516.60 ± 15% | 2.71 ± 7% | 29.05 ± 3% | 1656 ± 6% | 3.08 ± 6% |
| 4 | 10 | 1.2 | 80 | 26.30 ± 2% | 1596.88 ± 20% | 2.46 ± 7% | 30.56 ± 3% | 1851 ± 2% | 2.26 ± 3% |
| 5 | 0 | 0.8 | 100 | 52.82 ± 3% | 3129.44 ± 8% | 2.50 ± 11% | 55.09 ± 1% | 2877.6 ± 2% | 3.53 ± 8% |
| 6 | 10 | 0.8 | 100 | 43.71 ± 3% | 2738.50 ± 5% | 2.75 ± 5% | 50.29 ± 6% | 2760 ± 2% | 3.35 ± 5% |
| 7 | 0 | 1.2 | 100 | 48.88 ± 4% | 2341.39 ± 12% | 2.56 ± 5% | 67.42 ± 3% | 3429.6 ± 5% | 3.06 ± 6% |
| 8 | 10 | 1.2 | 100 | 45.36 ± 2% | 3020.67 ± 3% | 2.18 ± 5% | 66.12 ± 5% | 3606 ± 3% | 2.75 ± 7% |
| 9 | 5 | 1 | 90 | 36.76 ± 4% | 2387.95 ± 4% | 2.26 ± 9% | 47.05 ± 7% | 2168.7 ± 8% | 3.42 ± 10% |

Table 5 Regression equations of strength, elastic modulus, and strain obtained with the tension and bending tests and goodness of fit (R^2 predicted)

| Tensile regression equations | R^2 -pred |
|--|-------------|
| σ_t (MPa) = $-177.3 + 8.57 \cdot G + 107.9 \cdot NS + 2.381 \cdot I - 7.32 \cdot G \cdot NS - 0.106 \cdot G \cdot I - 1.178 \cdot NS \cdot I + 0.0872 \cdot G \cdot NS \cdot I$ | 98.55% |
| ϵ_t (%) = $3.633 + 0.1572 \cdot G + 0.065 \cdot NS - 0.01251 \cdot I - 0.1576 \cdot G \cdot NS$ | 31.80% |
| E_t (MPa) = $-14592 + 954 \cdot G + 10675 \cdot NS + 193.3 \cdot I - 989 \cdot G \cdot NS - 12.10 \cdot G \cdot I - 126.5 \cdot NS \cdot I + 12.60 \cdot G \cdot NS \cdot I$ | 87.42% |
| Bending regression equations | R^2 -pred |
| σ_f (MPa) = $158.6 + 2.094 \cdot G - 236.5 \cdot NS - 1.304 \cdot I - 0.02474 \cdot G \cdot I + 2.696 \cdot NS \cdot I$ | 97.85% |
| ϵ_f (%) = $26.35 + 0.0453 \cdot G - 20.11 \cdot NS - 0.2198 \cdot I - 0.0871 \cdot G \cdot NS + 0.1910 \cdot NS \cdot I$ | 90.54% |
| E_f (MPa) = $-1610 - 48.3 \cdot G - 3145 \cdot NS + 32.7 \cdot I + 54.9 \cdot G \cdot NS + 46.0 \cdot NS \cdot I$ | 97.46% |

G (%) glass percentage added to the mixture, I (%) infill density during printing, NS (mm) refers to the nozzle size

II. The other reason lies in the properties acquired by the material due to the extrusion process itself. It has been found, using commercial filaments, that in the tension test a more extensive creep zone appears in comparison with those obtained in the laboratory with filaments manufactured using the 3DEVO extruder. In other words, the filaments manufactured in the laboratory show a more fragile behaviour. One of the reasons for this change in plastic zone properties could be attributed to differences in the cooling method. While the desktop extruder 3DEVO is cooled with the help of two small fans focused at the outlet of the extrusion nozzle, the commercial filaments used are cooled by water pools of several meters, the cooling being more gradual. Related to the extrusion process, differences also could be allocated to the use of plasticisers by commercial filament manufacturers. However, this could not be corroborated as the manufacturers keep the composition of their blends confidential.

In the case of the bending regression equations, adequate fits were obtained for the three mechanical parameters, with good predictability, always greater than 90%.

Another way to analyze the DoE results is the interpretation of Pareto diagrams (Fig. 3). These shows, in decreasing order, which terms in the model are influential. It also details which are statistically significant, i.e., when their standardised effect is above the red line, which marks the quantile $(1-\alpha/2)$, where $\alpha=0.05$ represents the significance level: the probability of rejecting the null hypothesis when it is true.

In the tensile modulus of elasticity as well as in the tensile and flexural strengths, the most influential parameter is the infill density. In the flexural modulus of elasticity, the infill density is the second most important parameter. In addition, nozzle size and glass percentage also have an influence on these 4 output variables, although with different importance and not in all cases they are statistically significant terms. While for tensile strength and modulus 7 terms (independent and interactions) are needed to define

these output variables, for modulus and flexural strength 5 terms are sufficient.

The strain at the point of maximum strength in tension is approximated by 4 terms and in bending by 5. However, there is no unanimity in the order of importance of the terms, observing for example that in tension the percentage of the glass has a minimal influence while in bending it has a greater relevance in the result, although it continues to be the least influential independent factor.

As to whether the influence of these terms is directly or inversely proportional to the mechanical parameters, it is necessary to study the main effects of each term (Table 6). The effect of a factor, which calculates the change when the factor varies from its low to high level, is used to represent the expected change in the mean response. The sign of the effect indicates the direction of the relationship between the term and the response. It is observed that the interaction of nozzle size and infill density influences in all tensile and bending mechanical properties with the exception of tensile strain. Furthermore, this term has a directly proportional influence on bending parameters, while in tension it is inversely proportional. It is also noteworthy that precisely the strain corresponding to the maximum tensile strength has the worst goodness-of-fit (predicted R^2). Interestingly, for the maximum strength in both tension and bending, the single most influential parameter is the infill density, implying higher strength values with the increase of infill density. As for the terms with interactions, the most influential is the nozzle size with the infill density in bending, while in tension it is also the nozzle size but this time interacting with the percentage of glass load. Again, an increase in each term has a positive effect in the mentioned output.

3.3 LCA

A cradle-to-gate LCA was carried out for the nine alternatives under study. The functional unit considered for this analysis is 1 kg of printable material with different proportions of PLA and glass powder according to Table 1.

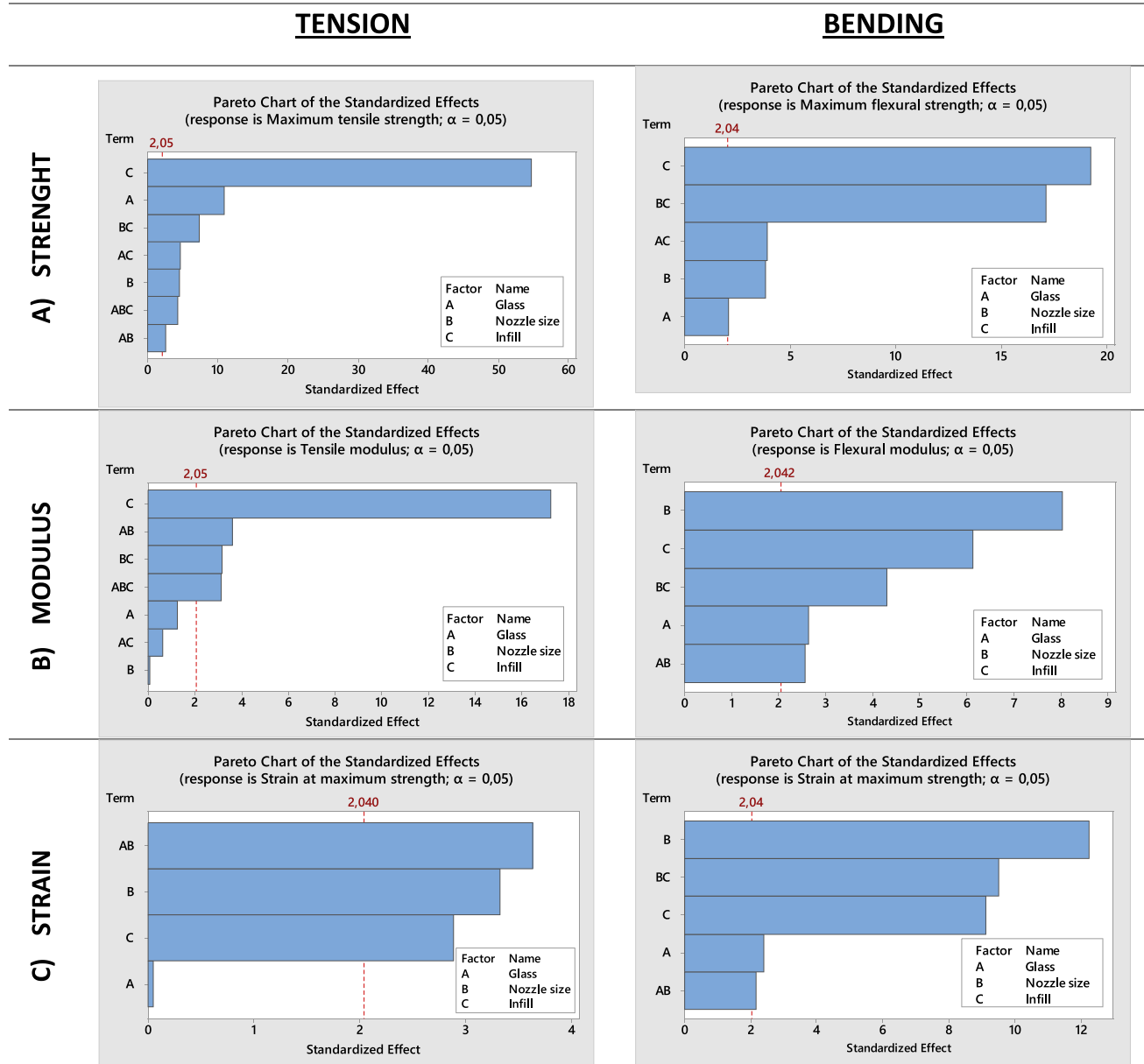


Fig. 3 Pareto charts for the two types of tests (tension and bending) and the three output variables (strength, elastic modulus, and strain)

Table 6 Main effects of each term of the models for the three output variables of tension and bending tests. Terms could be the independent input variables, the interaction two by two of the interaction of the three

| Term | Tension | | | Bending | | |
|------------|---------|---------|------------------|---------|---------|------------------|
| | Modulus | Strain | Maximal strength | Modulus | Strain | Maximal strength |
| G | 100.3 | -0.0045 | -4.429 | 90.5 | -0.156 | -0.0532 |
| Ns | 7.0 | -0.2891 | 1.822 | 10,504 | -30.1 | 60.7 |
| I | 1387.9 | -0.2502 | 22.177 | 5255 | 14.706 | 243 |
| G · NS | 289.2 | -0.3152 | 1.056 | 109.8 | -0.1741 | - |
| G · I | 49.9 | - | -1.882 | - | - | -0.099 |
| NS · I | -253.8 | - | -2.967 | 4600 | 19.1 | 269.57 |
| G · NS · I | 252.0 | - | 1.744 | - | - | - |

The life cycle inventory of the PLA was obtained from Ecoinvent 3.0 database (market for polylactide, granulate (GLO), cut-off, U). This dataset includes the PLA production process and also the trade between the producer and consumer, being the transportation process also considered.

As for the glass powder, it is a by-product obtained from the recycling of windshields. Two main processes are involved in vehicle glass recycling: the dismantling and the processing of the windshields (Table 7). The first one, dismantling, consists of removing the windshields from the car. The electricity and diesel consumption during this process have been obtained from [41], and it is summarized in Table 7 per ton of glass powder. According to it, an electric cutter of 1 kW for 2 min can be used to separate the windshields that are glued to the vehicle’s structure. The rest can be separated by manual force. In addition, a forklift is used to transport the vehicle within the installations (0.2 l of

diesel per vehicle). For the dismantling process, 0.031 tons glass per vehicle has been estimated. Finally, the obtained windshields are transported to the recycling plant. An average transportation distance of 50 km has been considered.

The second one, windshields processing, consists of two main steps: crushing and hammer milling. The first step uses, for a production of 30-ton glass per hour, 54 l of diesel for both a shredder and a wheel loader and 15 kWh electricity for the conveyors and other electrical equipment [41]. The second step with a capacity of 8 ton/h, consumes around 48 kWh [41]. From the total input of the windshield processing, it is estimated that 65% is glass and around 30% of the glass is glass powder.

The environmental profile of the alternatives is expressed considering 16 impact categories, following the impact assessment method of the Environmental Footprint initiative, the EF method 3.0 normalization, and weighting set [42]. The results are shown in Table 8. In bold, the total EF on the different cases resulting from the sum of all the categories detailed in the previous rows.

Finally, for the transportation of glass powder to the consumer, a transportation distance of 100 km has been assumed. The Ecoinvent dataset for a lorry (3.5–7.5 tons, Euro 4) has been chosen.

Among the different printing materials, those with the highest percentage of glass powder present the lowest global

Table 7 Diesel and electricity consumption for the production of 1 ton of glass powder from end-of-life windshields

| | Dismantling | Windshield processing | |
|-----------------------|-------------|-----------------------|-------------|
| | | Shredding | Hammer mill |
| Diesel (l/ton) | 9.7 | 2.8 | 0.4 |
| Electricity (kWh/ton) | 0.6 | 0.8 | 9.2 |

Table 8 LCA analysis

| Category of impact | Units | Characterization (EF 3.0) | | | Normalized and weighted (EF3.0) | | |
|-----------------------------------|--------------|---------------------------|--------------------|----------|---------------------------------|--------------------|---------------|
| | | Cases 1, 3, 5, & 7 | Cases 2, 4, 6, & 8 | Case 9 | Cases 1, 3, 5, & 7 | Cases 2, 4, 6, & 8 | Case 9 |
| Climate change | kg CO2 eq | 3.15E+00 | 2.84E+00 | 2.99E+00 | 81.83 | 73.93 | 77.88 |
| Ozone depletion | kg CFC11 eq | 2.36E-07 | 2.14E-07 | 2.25E-07 | 0.28 | 0.25 | 0.26 |
| Ionising radiation | kBq U-235 eq | 2.48E-01 | 2.24E-01 | 2.36E-01 | 2.94 | 2.66 | 2.80 |
| Photochemical ozone formation | kg NMVOC eq | 1.18E-02 | 1.07E-02 | 1.13E-02 | 13.94 | 12.65 | 13.29 |
| Particulate matter | disease inc | 1.56E-07 | 1.42E-07 | 1.49E-07 | 23.50 | 21.38 | 22.44 |
| Human toxicity, non-cancer | CTUh | 5.56E-08 | 5.02E-08 | 5.29E-08 | 4.46 | 4.02 | 4.24 |
| Human toxicity, cancer | CTUh | 2.15E-09 | 1.94E-09 | 2.04E-09 | 2.71 | 2.44 | 2.58 |
| Acidification | mol H+eq | 2.08E-02 | 1.88E-02 | 1.98E-02 | 23.26 | 21.02 | 22.14 |
| Eutrophication, freshwater | kg P eq | 1.17E-03 | 1.06E-03 | 1.12E-03 | 20.47 | 18.44 | 19.45 |
| Eutrophication, marine | kg N eq | 7.64E-03 | 6.91E-03 | 7.28E-03 | 11.58 | 10.46 | 11.02 |
| Eutrophication, terrestrial | mol N eq | 6.60E-02 | 5.97E-02 | 6.29E-02 | 13.86 | 12.54 | 13.20 |
| Ecotoxicity, freshwater | CTUe | 1.21E+02 | 1.09E+02 | 1.15E+02 | 54.28 | 48.91 | 51.59 |
| Land use | Pt | 3.54E+01 | 3.19E+01 | 3.36E+01 | 3.43 | 3.09 | 3.26 |
| Water use | m3 depriv | 4.38E+00 | 3.94E+00 | 4.16E+00 | 32.50 | 29.26 | 30.88 |
| Resource use, fossils | MJ | 3.89E+01 | 3.52E+01 | 3.70E+01 | 49.76 | 44.99 | 47.38 |
| Resource use, minerals and metals | kg Sb eq | 2.67E-05 | 2.41E-05 | 2.54E-05 | 31.68 | 28.56 | 30.12 |
| Total | | | | | 370.49 | 334.60 | 352.55 |

environmental impact. This is because the impact of recycling glass powder is lower than that of producing virgin PLA, so the substitution of the same amount of PLA by recycled glass powder results in a reduced environmental burden. Looking at each impact category individually, the behaviour is the same. The lower the amount of PLA, the lower the impact, being the reduction almost constant in all the category impact and around 10%.

3.4 Costs

The *filament cost* calculation (Table 9) involves the sum of the price of PLA, given by the company EOLAS Prints, and the glass powder that makes up the additive, given by FCC Ámbito S.A., as well as the extrusion of this material to obtain the filament that is used to print the parts. Cases on Table 9 are grouped by their similarity on their cost calculation, whose totals are marked in bold in the last row.

When calculating the extrusion cost using Eq. (1), C is obtained from the invoice in the purchase date (24/11/2021), SV , SL , and H_{annual} were estimated from data coming from other company’s experience, since the desktop extruder used has only been on the market for less than 5 years, and no specific data is available.

As for the *printing cost* (Table 10), the cost of the printer was obtained from the invoice in the purchase date (31/03/2021). Same reasoning as for the extruder applies for the calculation of SV , SL and H_{annual} . Labor cost was estimated by diving the average salary in Spain of a junior engineer (in €/h) by the average mass flow of each case, obtained at the laboratory. The electricity costs were calculated using a consumption value of 20 kWh, the average daily value is taken on 27/10/2022. In addition, the printing speed in kg/h is obtained for each case. As in table 9, cases

are grouped in table 10 by its calculation similarities. Values in bold indicate the total printing costs in €/kg, as a sum of the previous rows.

The results show that the cheapest filament is made in cases 1, 3, 5, and 7, which are the cases without glass powder. Despite the raw materials being cheaper in cases with glass, the extrusion costs increase due to the lower production speed. On the other hand, the lowest printing costs occur in cases 7 and 8, followed by 3 and 4, which are the cases that share a nozzle size of 1.2 mm, which means a lower printing time and consequently a decrease in all the items of the printing costs.

3.5 Results of the MCDMA

3.5.1 Criteria weighting

With the aim of giving weight to the criteria and minimizing the subjectivity of the decision, a survey, in which the alternatives are scored in line with the AHP methodology, was carried out. Researchers and employees of companies involved in 3D printing were consulted and a total of 10 results were obtained.

With the information from the surveys, and using AHP methodology, the following weights were obtained for each of the criteria:

- Filament cost: 0.155
- Printing cost: 0.378
- Environmental impact: 0.467

3.5.2 Initial decision matrices

For the generation of the initial decision matrices, the costs and the environmental impact per unit of mass were divided by the tensile or flexural strength in each case, so the two initial decision matrices were obtained (Tables 11 and 12), which were the starting point for the four multi-criteria analyses.

3.5.3 Final ranking of the alternatives

Applying the WASPAS and TOPSIS methodology described in Section 2.8.4, results are obtained and shown in Table 13 and Fig. 4.

Table 9 Filament costs in € per kg

| | Cases 1, 3, 5, and 7 | Cases 2, 4, 6, and 8 | Case 9 |
|-----------------------------------|----------------------|----------------------|--------------|
| PLA cost (€/kg) | 10.99 | 9.89 | 10.44 |
| Glass cost (€/kg) | - | 0.01 | 0.005 |
| Filament extrusion cost (€/kg) | 30.00 | 31.58 | 30.77 |
| Total filament cost (€/kg) | 40.99 | 41.48 | 41.21 |

Table 10 Printing costs in € per kg

| | Cases 1 and 2 | Cases 3 and 4 | Cases 5 and 6 | Cases 7 and 8 | Case 9 |
|---|---------------|---------------|---------------|---------------|---------------|
| Depreciation and maintenance costs (€/kg) | 3.26 | 2.36 | 3.14 | 2.27 | 2.68 |
| Labor costs (€/kg) | 371.86 | 268.59 | 357.95 | 258.73 | 305.56 |
| Electricity cost (€/kg) | 3.06 | 2.21 | 2.98 | 2.15 | 2.53 |
| Total printing costs (€/kg) | 378.19 | 273.16 | 364.07 | 263.15 | 310.81 |

Table 11 Initial decision matrix of the MCDMA considers the tension strength as the normalized factor

| Alternatives | Tension | | |
|--------------|---------------------------|---------------------------|-----------------------------------|
| | Filament costs (€/KG)/MPA | Printing costs (€/KG)/MPA | Environmental impact (LCA/KG)/MPA |
| Case 1 | 1.704 | 15.725 | 15.405 |
| Case 2 | 1.869 | 17.043 | 15.079 |
| Case 3 | 1.388 | 9.250 | 12.546 |
| Case 4 | 1.577 | 10.386 | 12.722 |
| Case 5 | 0.776 | 6.893 | 7.014 |
| Case 6 | 0.949 | 8.329 | 7.655 |
| Case 7 | 0.839 | 5.384 | 7.580 |
| Case 8 | 0.914 | 5.801 | 7.377 |
| Case 9 | 1.121 | 8.455 | 9.591 |

Table 12 Initial decision matrix of the MCDMA considering the bending strength as the normalized factor

| Alternatives | Bending | | |
|--------------|---------------------------|---------------------------|-----------------------------------|
| | Filament costs (€/KG)/MPA | Printing costs (€/KG)/MPA | Environmental impact (LCA/KG)/MPA |
| Case 1 | 1.084 | 10.000 | 9.796 |
| Case 2 | 1.076 | 9.810 | 8.680 |
| Case 3 | 1.411 | 9.403 | 12.754 |
| Case 4 | 1.357 | 8.938 | 10.949 |
| Case 5 | 0.744 | 6.609 | 6.725 |
| Case 6 | 0.825 | 7.240 | 6.653 |
| Case 7 | 0.608 | 3.903 | 5.495 |
| Case 8 | 0.627 | 3.980 | 5.060 |
| Case 9 | 0.876 | 6.606 | 7.493 |

The rankings of the WASPAS technique are equal to those obtained via TOPSIS. This implicates that the conclusions of both methods are identical. Depending on the strength used as a normalizing factor (tension or bending),

Table 13 Results and ranking of the cases subjected to WASPAS and TOPSIS methodology

| Alternatives | Tension WASPAS | | Tension TOPSIS | | Bending WASPAS | | Bending TOPSIS | |
|--------------|----------------|------|----------------|------|----------------|------|----------------|------|
| | Qi | Rank | Pi | Rank | Qi | Rank | Pi | Rank |
| Case 1 | 0.411 | 8 | 0.0890 | 8 | 0.473 | 7 | 0.2967 | 7 |
| Case 2 | 0.398 | 9 | 0.0241 | 9 | 0.506 | 6 | 0.3903 | 6 |
| Case 3 | 0.568 | 6 | 0.5249 | 6 | 0.409 | 9 | 0.0537 | 9 |
| Case 4 | 0.529 | 7 | 0.4588 | 7 | 0.450 | 8 | 0.2096 | 8 |
| Case 5 | 0.914 | 3 | 0.9062 | 3 | 0.698 | 3 | 0.7029 | 3 |
| Case 6 | 0.794 | 4 | 0.8071 | 4 | 0.669 | 4 | 0.6637 | 4 |
| Case 7 | 0.953 | 1 | 0.9564 | 1 | 0.963 | 2 | 0.9556 | 2 |
| Case 8 | 0.926 | 2 | 0.9523 | 2 | 0.988 | 1 | 0.9910 | 1 |
| Case 9 | 0.689 | 5 | 0.7161 | 5 | 0.646 | 5 | 0.6405 | 5 |

the order of the alternatives changes. The best options are distributed between cases 7 and 8. Both cases are 100% filled and use a nozzle size of 1.2 mm, and their difference lies in the material, with pure PLA prevailing when normalised for tensile strength, and a glass filler of 10% in weight added to PLA when normalised for flexural strength. In third place is case 5 in both analyses.

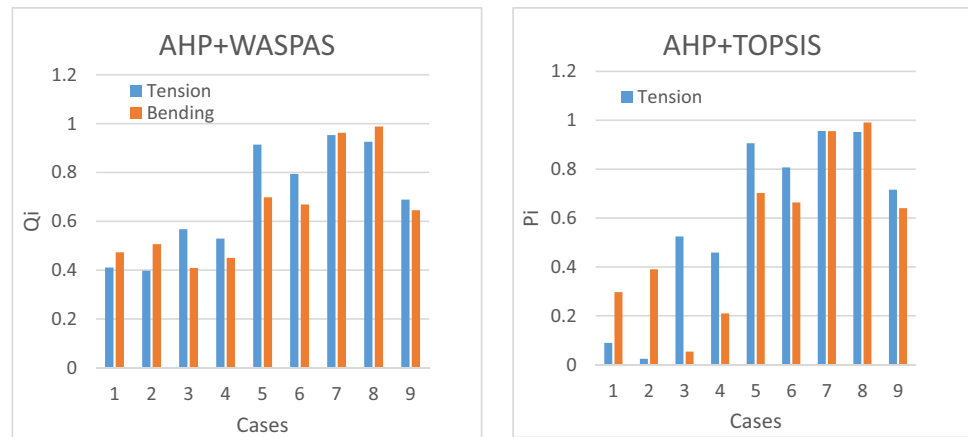
For both tension and bending stress, the first four places in the ranking are assigned to alternatives with 100% infill. The fifth place goes to case 9 with 90% infill and the last places in the ranking go to cases with 80% infill. This means that the amount of material is a factor with a great influence on the decision-making, but the reduction in strength is not proportional to the reduction in the amount of material used. Otherwise, there should not be such an appreciable difference between the Qi values with 100% infill and those with 80% infill.

Finally, it is worth highlighting the relevance of the use of the two MCDMA for the determination of the cases with the best characteristics. Taking the tensile strength of the material as the only decision-making criterion, the best possible alternative would have been case 5 with a strength of 52.82 MPa. This alternative has 100% PLA, 100% infill, and a nozzle size of 0.8 mm. This last characteristic, nozzle size, does not correspond to the winning alternatives of the MCDMA, because its influence on the printing time, and therefore on the cost, has a negligible impact.

4 Conclusions

In this work, the infill density, nozzle size, and the addition of glass powder that influence the mechanical properties (tension and bending) have been analyzed using fused deposition modeling. For this purpose, a design of experiments was used from which regression equations of the mechanical properties for tensile and flexural parameters were obtained with high percentages of reliability. The output variables are the maximum strength, the deformation corresponding to the maximum strength, and the elastic modulus. It is shown

Fig. 4 Performance comparison of alternatives 1 to 9 normalizing the criteria by tension strength or by bending strength using AHP + WASPAS (left), or AHP + TOPSIS (right)



that the three input parameters individually influence all the mechanical properties. The interaction between the nozzle size and the infill density influences all models except the deformation corresponding to the maximum tensile strength, although it is precisely the one with the lowest accuracy. This interaction has a positive influence on the flexural properties while in tensile properties it is negative. In both tensile and flexural strength, the term with the greatest influence is the infill density of the part.

Although intuitively it could be thought that the strength has a proportional relation with the infill density, it has been demonstrated that the other two parameters analyzed, among others, also influence the mechanical behavior and affect this relationship, i.e., models with 80% infill do not give a strength equal to 80% of that obtained in completely solid specimens.

The economic study was divided in filament and printing costs. For the first category, the lowest values were obtained in those cases without glass powder, and the second one for those that share the largest nozzle size (1.2-mm diameter).

As for the environmental performance, the partial substitution of PLA by waste glass powder in the printing material seems to reduce its environmental impact.

To facilitate the decision-making among the nine cases studied, a multi-criteria analysis has been performed, considering filament costs, printing costs, and environmental impact. Due to structural function purpose of the parts built with these materials, all values have been normalized by tensile and flexural strength, respectively. The assessment of the alternatives using WASPAS gave the same rankings as those using TOPSIS. These analyses show that in case of uniaxial stresses the most suitable option is case 7 (0% glass powder, 1.2-mm nozzle size, and 100% infill). Nevertheless, pieces manufactured by 3D printing are not only subjected to uniaxial stresses but also to combined stresses, resembling a flexural behavior, since tensile and compressive loads as well as shear stresses between the layers appear. Considering flexural stress, the most suitable alternative is

case 8 (10% glass powder, 1.2-mm nozzle size, and 100% infill).

Since there is no agreement between the standardized multi-criteria analyses for tensile and flexural strengths, respectively, it is up to the worker to decide which is the best alternative, considering the type of stresses to which the piece to be manufactured will be subjected.

Acknowledgements The authors want to thank the following entities for their contribution: LAGUC laboratory, for providing the equipment to carry out the mechanical tests and FCC Ámbito, for providing the crushed recycled glass.

Author contribution All authors contributed to the study conception and design. Material preparation and data collection were performed by Paula Palomera-Obregon and Irune Indacoechea-Vega. Analysis was done by all the authors. The first draft of the manuscript was written by Laura Castanon-Jano and all authors commented on previous versions of the manuscript. All authors read and approved the final manuscript.

Funding Open Access funding provided thanks to the CRUE-CSIC agreement with Springer Nature. This work has been co-financed by the Spanish Ministry of Science and Innovation through the R + D + i projects 2020 call, under the project “Fostering the circular economy and low CO₂ technologies through the additive manufacturing (3DCircle).” (PID2020-112851RA-I00).

Declarations

Ethics approval This article does not contain any studies with human or animal subjects performed by any of the authors.

Consent for publication All the authors have given their consent for publication of this manuscript.

Competing interests The authors declare no competing interests.

Disclaimer This work reflects the authors’ opinion, so the authorities of the programme are not responsible for the use of the information here included.

Open Access This article is licensed under a Creative Commons Attribution 4.0 International License, which permits use, sharing, adaptation, distribution and reproduction in any medium or format, as long as you give appropriate credit to the original author(s) and the source,

provide a link to the Creative Commons licence, and indicate if changes were made. The images or other third party material in this article are included in the article's Creative Commons licence, unless indicated otherwise in a credit line to the material. If material is not included in the article's Creative Commons licence and your intended use is not permitted by statutory regulation or exceeds the permitted use, you will need to obtain permission directly from the copyright holder. To view a copy of this licence, visit <http://creativecommons.org/licenses/by/4.0/>.

References

- Chen J, Liu X, Tian Y, Zhu W, Yan C, Shi Y, Kong LB, Qi HJ, Zhou K. (2021) 3D-printed anisotropic polymer materials for functional applications. *Advanced Materials* 4(5):2102877 <https://doi.org/10.1002/adma.202102877>
- Lalegani Dezaki M, Bodaghi M, Serjouei A, Zolfagharian A (2023) Green 3D-printed lattice-shaped suspension arms for RC cars. *Prog Addit Manuf.* <https://doi.org/10.1007/s40964-023-00439-2>
- Bouzaglou O, Golan O, Lachman N (2023) Process design and parameters interaction in material extrusion 3D printing: a review. *Polymers (Basel)* 15:2280. <https://doi.org/10.3390/polym15102280>
- Gebisa AW, Lemu HG (2019) Influence of 3D printing FDM process parameters on tensile property of ULTEM 9085. *Procedia Manuf* 30:331–338. <https://doi.org/10.1016/j.promfg.2019.02.047>
- Lokesh N, Reddy JS, Praveen BA, Kishore Veeresh YM, Sreehari Acharya B, Eshwar Kapse J, Pramath P, Nadig PP, Prasad M (2023) Evaluation and optimization of process parameter for surface roughness of 3D-printed PETG specimens using Taguchi method at constant printing temperature. *Lecture Notes in Mechanical Engineering* 201–212. https://doi.org/10.1007/978-981-16-9057-0_22
- Mishra SB, Acharya E, Banerjee D, Khan MS (2019) An experimental investigation of surface roughness of FDM build parts by chemical misting. *IOP Conf Ser Mater Sci Eng* 653:012043. <https://doi.org/10.1088/1757-899X/653/1/012043>
- Mulcahy N, O'Sullivan KJ, O'Sullivan A, O'Sullivan L (2023) Preliminary assessment on the effects of line width, layer height and orientation on strength and print time for FDM printing of total contact casts for the treatment of diabetic foot ulcers. *Ann 3D Print Med* 11:100115. <https://doi.org/10.1016/j.stlm.2023.100115>
- Wang P, Zou B, Ding S (2019) Modeling of surface roughness based on heat transfer considering diffusion among deposition filaments for FDM 3D printing heat-resistant resin. *Appl Therm Eng* 161:114064. <https://doi.org/10.1016/j.applthermaleng.2019.114064>
- Kumar K, Singh H (2023) Multi-objective optimization of fused deposition modeling for mechanical properties of biopolymer parts using the Grey-Taguchi method. *Chin J Mech Eng* 36:30. <https://doi.org/10.1186/s10033-023-00847-z>
- Solomon IJ, Sevel P, Gunasekaran J (2021) A review on the various processing parameters in FDM. *Mater Today Proc* 37:509–514. <https://doi.org/10.1016/j.matpr.2020.05.484>
- Ding S, Zou B, Wang P, Ding H (2019) Effects of nozzle temperature and building orientation on mechanical properties and microstructure of PEEK and PEI printed by 3D-FDM. *Polym Test* 78:105948. <https://doi.org/10.1016/j.polymertesting.2019.105948>
- Ouazzani K, El Jai M, Akhrif I et al (2023) An experimental study of FDM parameter effects on ABS surface quality: roughness analysis. *Int J Adv Manuf Technol* 127:151–178. <https://doi.org/10.1007/s00170-023-11435-9>
- Le C, Kolasangiani K, Nayyeri P, Bougherara H (2023) Experimental and numerical investigation of 3D-printed bone plates under four-point bending load utilizing machine learning techniques. *J Mech Behav Biomed Mater* 143:105885. <https://doi.org/10.1016/j.jmbbm.2023.105885>
- Rodríguez-Panes A, Claver J, Camacho AM (2018) The influence of manufacturing parameters on the mechanical behaviour of PLA and ABS pieces manufactured by FDM: a comparative analysis. *Materials* 11:1333. <https://doi.org/10.3390/MA11081333>
- Bembenek M, Kowalski Ł, Kosoń-Schab A (2022) Research on the influence of processing parameters on the specific tensile strength of FDM additive manufactured PET-G and PLA materials. *Polymers (Basel)* 14:2446. <https://doi.org/10.3390/polym14122446>
- Ilyas RA, Sapuan SM, Harussani MM et al (2021) Poly(lactic acid) (PLA) biocomposite: processing, additive manufacturing and advanced applications. *Polymers (Basel)* 13:1326. <https://doi.org/10.3390/polym13081326>
- Vakharia VS, Kuentz L, Salem A et al (2021) Additive manufacturing and characterization of metal particulate reinforced poly(lactic acid) (PLA) polymer composites. *Polymers (Basel)* 13:3545. <https://doi.org/10.3390/POLYM13203545>
- Vu MC, Jeong TH, Kim JB et al (2021) 3D printing of copper particles and poly(methyl methacrylate) beads containing poly(lactic acid) composites for enhancing thermomechanical properties. *J Appl Polym Sci* 138:49776. <https://doi.org/10.1002/APP.49776>
- Jiang D, Ning F, Wang Y (2021) Additive manufacturing of biodegradable iron-based particle reinforced polylactic acid composite scaffolds for tissue engineering. *J Mater Process Technol* 289:116952. <https://doi.org/10.1016/j.jmatprotec.2020.116952>
- Lee J, Lee H, Cheon KH et al (2019) Fabrication of poly(lactic acid)/Ti composite scaffolds with enhanced mechanical properties and biocompatibility via fused filament fabrication (FFF)-based 3D printing. *Addit Manuf* 30:100883. <https://doi.org/10.1016/j.addma.2019.100883>
- Song X, He W, Han X, Qin H (2020) Fused deposition modeling of poly (lactic acid)/nutshells composite filaments: effect of alkali treatment. *J Polym Environ* 28:3139–3152. <https://doi.org/10.1007/S10924-020-01839-Z>
- Song X, He W, Chen P et al (2021) Fused deposition modeling of poly (lactic acid)/almond shell composite filaments. *Polym Compos* 42:899–913. <https://doi.org/10.1002/PC.25874>
- Razali MS, Khimeche K, Melouki R et al (2022) Preparation and properties enhancement of poly(lactic acid)/calcined-seashell biocomposites for 3D printing applications. *J Appl Polym Sci* 139:51591. <https://doi.org/10.1002/APP.51591>
- Suárez L, Domínguez M (2020) Sustainability and environmental impact of fused deposition modelling (FDM) technologies. *Int J Adv Manuf Technol* 106:1267–1279. <https://doi.org/10.1007/s00170-019-04676-0>
- Anandkumar R, Ramesh Babu S, Sathyamurthy R (2021) Investigations on the mechanical properties of natural fiber granulated composite using hybrid additive manufacturing: a novel approach. *Adv Mater Sci Eng* 2021:5536171. <https://doi.org/10.1155/2021/5536171>
- Petchwattana N, Channuan W, Naknaen P, Narupai B (2019) 3D printing filaments prepared from modified poly(lactic acid)/teak wood flour composites: an investigation on the particle size effects and silane coupling agent compatibilisation. *J Phys Sci* 30:169–188. <https://doi.org/10.21315/JPS2019.30.2.10>
- Barba E, Mietner JB, Navarro JRG (2023) Grafting of poly(stearyl acrylate) on cellulose fibers as 3D-printable HDPE composites. *Cellulose* 30:2267–2278. <https://doi.org/10.1007/s10570-022-05021-7>
- Olesik P, Godzisz M, Koziol M (2019) Preliminary characterization of novel LDPE-based wear-resistant composite suitable for FDM 3D printing. *Materials* 12:2520. <https://doi.org/10.3390/MA12162520>
- Olesik P, Koziol M, Konik D, Jała J (2019) The use of shredded car windscreens waste as reinforcement of thermoplastic composites for 3D (FDM) printing. *Compos Theory Pract* 19:30–33
- Kristiawan RB, Imaduddin F, Ariawan D et al (2021) A review on the fused deposition modeling (FDM) 3D printing: filament

- processing, materials, and printing parameters. *Open Eng* 11:639–649. <https://doi.org/10.1515/eng-2021-0063>
31. Algarni M, Ghazali S (2021) Comparative study of the sensitivity of PLA, ABS, PEEK, and PETG's mechanical properties to FDM printing process parameters. *Crystals (Basel)* 11:995. <https://doi.org/10.3390/CRYST11080995>
 32. Alsoufi MS, Elsayed AE (2017) How surface roughness performance of printed parts manufactured by desktop FDM 3D printer with PLA+ is influenced by measuring direction. *Am J Mech Eng* 5:211–222. <https://doi.org/10.12691/AJME-5-5-4>
 33. Ferretti P, Leon-Cardenas C, Santi GM et al (2021) Relationship between FDM 3D printing parameters study: parameter optimization for lower defects. *Polymers (Basel)* 13:2190. <https://doi.org/10.3390/POLYM13132190>
 34. Ly O, Yoris-Nobile AI, Sebaibi N et al (2021) Optimisation of 3D printed concrete for artificial reefs: biofouling and mechanical analysis. *Constr Build Mater* 272:121649. <https://doi.org/10.1016/J.CONBUILDMAT.2020.121649>
 35. Boukhelf F, Sebaibi N, Boutouil M et al (2022) On the properties evolution of eco-material dedicated to manufacturing artificial reef via 3D printing: long-term interactions of cementitious materials in the marine environment. *Sustainability* 14:9353. <https://doi.org/10.3390/SU14159353>
 36. UNE-EN ISO 527–1:2020 Plásticos. Determinación de las propiedades en tracción. Parte 1: Principios generales. International Organization for Standardization. Accessed 2 Nov 2022
 37. UNE-EN ISO 178:2020 Plásticos. Determinación de las propiedades de flexión. International Organization for Standardization. Accessed 2 Nov 2022
 38. Saaty TL (1980) *The analytic hierarchy process: planning, priority setting, resource allocation*. MacGraw-Hill, New York International Book Company
 39. Zavadskas EK, Turskis Z, Antucheviciene J, Zakarevicius A (2012) Optimization of weighted aggregated sum product assessment. *Elektronika ir Elektrotechnika* 122:3–6. <https://doi.org/10.5755/J01.EEE.122.6.1810>
 40. Hwang C-L, Yoon K (1981) *Methods for multiple attribute decision making*. Lecture Notes in Economics and Mathematical Systems. Springer, Berlin, Heidelberg, pp 58–191
 41. Lassesson H (2008) *Energy consumptions and CO2 emissions resulting from different handling strategies of glass from end-of-life vehicles*. Master of Science Thesis. Chalmers University of Technology. Göteborg, Sweden
 42. Fazio S, Biganzoli F, De Laurentiis V, Zampori L, Sala S, Diaconu E (2018) Supporting information to the characterisation factors of recommended EF Life Cycle Impact Assessment methods, EUR 29600 EN, Publications Office of the European Union, Luxembourg. <https://doi.org/10.2760/002447>
- Publisher's note** Springer Nature remains neutral with regard to jurisdictional claims in published maps and institutional affiliations.